energies

MDPI

Article

Effect of Clay Content on the Mechanical Properties of Hydrate-Bearing Sediments during Hydrate Production via Depressurization

Dongliang Li [1,2], Zhe Wang [1,2,3], Deqing Liang [1,2,*] and Xiaoping Wu [4,5]

1 Key Laboratory of Gas Hydrate, Guangzhou Institute of Energy Conversion, Chinese Academy of Sciences, Guangzhou 510640, China
2 Guangdong Provincial Key Laboratory of New and Renewable Energy Research and Development, Guangzhou 510640, China
3 Nano Science and Technology Institute, University of Science and Technology of China, Suzhou 215123, China
4 School of Earth & Space Science, University of Science and Technology of China, Hefei 230026, China
5 CAS Center for Excellence in Comparative Planetology, Hefei 230026, China
* Correspondence: liangdq@ms.giec.ac.cn; Tel.: +86-20-8705-7657; Fax: +86-20-8705-7669

Received: 11 June 2019; Accepted: 11 July 2019; Published: 12 July 2019

Abstract: The effects of sediments with different clay contents on the mechanical properties of hydrate deposits were studied using a high-pressure, low-temperature triaxial apparatus with in-situ synthesis, as well as the mechanical properties of self-developed hydrate sediments. Through multi-stage loading, triaxial compression tests were conducted by adding quartz sand with different clay contents as the sediment skeleton, and the stress–strain relationship of the shearing process and the strength of sediments with different clay contents were determined. Volumetric changes were also observed during shearing. The results show that the strength of hydrate sediments decreases with the increasing clay content of sediments; in the processes of depressurization and shearing, the hydrate samples exhibited obvious shear shrinkage, regardless of the sediment particle size.

Keywords: triaxial shear; methane hydrate; clay content; mechanical property; hydrate mining; shear shrinkage

1. Introduction

The demand for energy in various countries is increasing with the continued development of modern society. The resources of traditional fossil fuels have diminished due to years of exploitation and utilization, and the world is facing an increasingly severe energy crisis. The natural gas hydrates that have been discovered thus far offer potential energy sources with which fossil fuels may be replaced. Natural gas hydrates are generally formed in low-temperature and high-pressure environments, and are mainly stored on deep-sea slopes and in permafrost regions [1,2]. Gas hydrates, primarily composed of methane, are naturally distributed across various regions worldwide. Because their shapes are similar to those of ice, they are often called "combustible ice." According to one survey, the reserves of natural gas hydrates may be 2.1×10^{16} m^3, and the decomposition of methane hydrates at approximately one atmosphere can produce ~160 m^3 of methane gas and ~0.87 m^3 of free water [3]. It is estimated that this is roughly twice as much as all carbonaceous fossil fuel reserves in the world [4].

Methane hydrate has attracted worldwide attention due to its wide distribution, large scale development, and high energy storage density. Extensive research on hydrates has been conducted in China, the United States, Japan, Canada, and other countries. At present, the methane hydrate mining methods proposed primarily include injection [5], pressure reduction [6], chemical reagents, and CO_2

replacement [7]. During the mining process, artificially breaking the stable conditions of the hydrate will cause it to decompose. Studies have shown that hydrates are cemented between sediments, which enhances the strength of seafloor sediments. In the process of hydrate mining, the hydrate will gradually decompose, the cementation and filling of the hydrate will be reduced, and the bearing capacity of the bottom layer will be greatly reduced. This may cause a series of geological disasters, if occurring at the bottom of the sea, including large tsunami and submarine landslides [8,9]. Therefore, it is very important to study the mechanical properties of hydrate-bearing sediments.

Since methane hydrates are mainly distributed in the deep sea and in permafrost regions, the cost of obtaining in-situ hydrated sediment cores for research is high and poses technical difficulties. Therefore, laboratory-synthesized gas hydrates are currently used as samples to study the relevant properties and various parameters of natural hydrates. The mechanical properties of hydrate sediments are mainly affected by hydrate saturation, confining pressure, sediment particle size, and sediment type. Researchers worldwide have performed studies on some of these properties. Winters et al. [10,11] used stored sand to study the effects of sediment type and porosity on hydrate sediments., and Hyodo et al. [12–14] used in-situ synthesis and mixed sample preparation methods to study the sedimentation, temperature, hydrate formation states (e.g., gas saturation formation, water saturation generation), and other hydrate formations in different sediments. The influence of mechanical properties indicates that the strength of hydrate sediments increases with the increase of hydrate saturation and confining pressure, and the strength of gas-saturated hydrate sediments is higher than that of other hydrate sediments under the same conditions. Moreover, Li et al. [15,16] studied the influence of hydrates on confining pressure and noted that the strength of hydrate sediments increased with the increase of confining pressure under certain conditions. Meanwhile, Song et al. [17,18] studied the effects of different temperatures and confining pressures on hydrate sediments. It is believed that under certain conditions, an increase in confining pressure will lead to an increase in the strength of hydrate sediments, as well as increases in temperature and shear rate, leading to an increase in shear strength.

Masui et al. [19] analyzed natural gas hydrates obtained from the South China Sea Trough in 2004 and synthesized matching hydrate sediment samples in the laboratory, with the original particle distribution, and distributed the two sets of samples for triaxial compression experiments. They concluded that the strengths of the natural and laboratory-synthesized hydrate sediments were consistent, and that the volume deformation characteristics were also the same. In order to study the effects of sand particle size on the mechanical properties of natural gas hydrate sediments, Miyazaki et al. [20] used Toyoura sand with three particle sizes as hydrate sediments, with median particle sizes (d50) of 0.230 mm, 0.205 mm, and 0.130 mm. The material skeleton was subjected to a drainage triaxial compression experiment under a constant temperature of 287 K. Their results showed that the strength of methane hydrate sediments increases with the saturation of hydrates and the effective confining pressure. Moreover, the strength of the hydrate sediments had little impact on the change in sand particle sizes, and the stiffness of the hydrate sediments was affected by the sand skeleton.

Kajiyama et al. [21] used circular glass beads and natural sand as the skeleton of methane hydrate deposits, and then performed a series of triaxial compression experiments on the two hydrate deposits to study their mechanical properties. The effects of particle characteristics on the mechanical properties of the methane-bearing hydrate sand were explained from the perspective of particle size. The stiffness of the glass bead skeleton and the reservoir sand was relatively uniform, but the maximum breaking strength was achieved in a short period of time. The apparent post-peak-strain softening behavior of the glass beads containing methane hydrate was observed experimentally. The main reason for the increase in the shear strength of the hydrate deposit with the glass bead skeleton was cohesion, but the shear strength of the natural sand containing methane hydrate was jointly controlled by the cohesive force and the internal angle of friction. This caused the strength of the methane hydrate deposit in the natural sand skeleton to increase with the increase of the effective confining pressure,

while the methane hydrate deposit in the glass bead skeleton had greater cohesion under relatively low pressures. In strong sediments and at higher effective confining pressures, cohesion will be greatly reduced due to the detachment of hydrates.

Hyodo et al. [14,22] used a self-made hydrate triaxial compression instrument to synthesize methane hydrate sediments using three grits with different densities as the methane sediment skeleton and by adding different contents of fine particles to the sand. They concluded that the addition of fine particles had a significant effect on the porosity of the sedimentary skeleton, and the fine particles filled in between the hydrate sediment skeletons, making the sample more compact and the initial porosity of the sample lower. Due to this lower porosity, the methane hydrate formed more severely hindered the movement of the particles, thereby increasing the strength of the entire methane hydrate sample. The porosity of the hydrate sediment samples was inversely proportional to the percentage of fine particles, and the strength of the hydrate sediments also increased. Additionally, the effects of fine particles on pure sand sediments and methane hydrate sediments differed. The presence of fine particles increased the strength of methane hydrate sediments and methane hydrates during triaxial shearing; meanwhile, dilatation occurred in the sediments, and pure sand sediments underwent shearing.

Many researchers have studied the mechanical properties of hydrate sediments. Most of this research has been focused on understanding the effects of sediments under single-variable conditions. However, fine-grained sediments host more than 90% of the accumulated global gas hydrates [23–25]; these accumulations of hydrate-bearing clayey sediments include those in the Gulf of Mexico, Krishna–Godavari Basin, Blake Ridge, Cascadia Margin, Ulleung Basin, Hydrate Ridge [26], and South China Sea [27]. Therefore, it is necessary to study the influence of clay content on the mechanical properties of sediments under multifactorial conditions. In this study, quartz sands with different proportions of clay were used as sediment skeletons, and the effects of clay content on the mechanical properties of hydrate sediments were studied using multi-stage loading triaxial compression tests combined with hydrate decomposition [28].

2. Materials and Methods

2.1. Experimental Apparatus

Figure 1 shows a schematic of the low-temperature, high-pressure triaxial apparatus used for the in-situ synthesis and mechanical property testing of self-developed hydrate sediments. The axial loading pressure ranged from 0–250 kN, the adjustable loading rate was 0.001–6 mm/min, and the three-axis pressure chamber (i.e., hydrate synthesis reactor) could set the confining pressure and pore pressure, ranging from 0–30 MPa. The sample size was Ø = 50 mm × 100 mm, the system operating temperatures were −30–50 °C (±0.5 °C), and the temperature range of the triaxial pressure chamber was approximately −30–50 °C (±0.5 °C). The device was mainly composed of a reaction kettle, a film-forming sediment preparation system, a stress loading system, a temperature control system, a confining pressure loading system, and a vacuum system. The temperature and pressure data during the experiment were monitored via computer in real time. The data acquisition rate of the computer reached up to 6 times per second, which could accurately monitor the temperature and pressure changes.

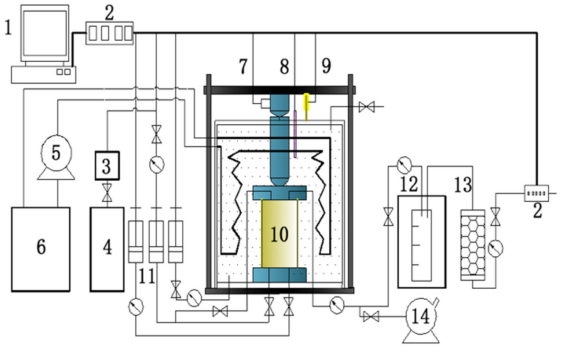

Figure 1. Schematic of the triaxial shear test apparatus: (**1**) computer; (**2**) data acquisition system; (**3**) buffer tank; (**4**) methane gas bottle; (**5**) water pump; (**6**) thermal control pump; (**7**) stress transducer; (**8**) temperature sensor; (**9**) displacement transducer; (**10**) specimen; (**11**) syringe pump; (**12**) gas–liquid separator; (**13**) desiccant; (**14**) vacuum pump [29].

2.2. Samples

The sand used in this experiment was a natural sand from the South China Sea. After screening with a 40–60 mesh sieve, deionized water was used to remove impurities, such as mud, ash, and salt. After preparation, the median grain size of the sand (d50) was found to be 377 μm, and the porosity was 33%; the grain size distribution of the sand is shown in Figure 2. The deionized water used in the experiment was made in the laboratory. The experimental clay was kaolin, for which the molecular formula is $Al_2Si_2O_9H_4$, and the relative molecular mass is 258.16.

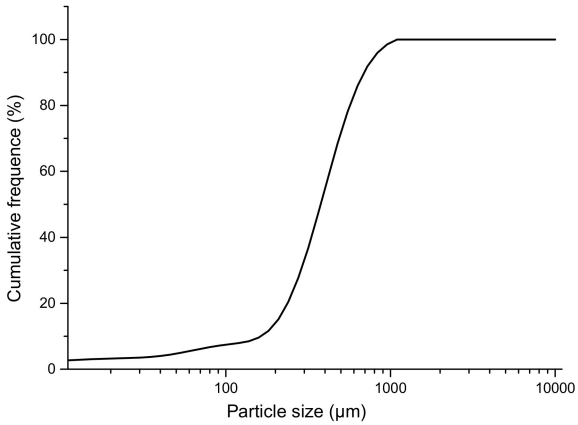

Figure 2. Grain size distribution curve.

2.3. Experimental Methods

Our experiments involved a multi-stage triaxial compression method [28], which is a repetitive loading triaxial compression shear test in soil mechanics. The same samples were used in the experiments to perform multi-stage shearing by changing the relevant parameters of the experiment. This method can effectively improve the experimental efficiency, as well as change the mechanical properties of hydrate sediment samples, in the case of changes in multiple experimental parameters.

2.3.1. Synthesis and Preparation of Samples

The sand used in the experiments was sieved and washed with deionized water, before being placed in an oven and allowed to stand at 104 °C for 10 h. After drying, a standardized amount of sand was placed into a plastic container, then the weighed clay was added in batches, and stirred simultaneously. After the mixture was almost uniform, the deionized water was added and stirred until

the agglomerated particles were invisible. The sand–clay mixture was then left to stand under closed conditions for 24 h, so that the deionized water was evenly distributed among the sand grains. A rubber mold with a thickness of 0.8 mm was fixed to the base of the test bench, and then a water-permeable plate, a stainless steel metal mesh, and a fast filter paper were sequentially placed at the bottom. The metal mold was fixed outside of the rubber mold with a rubber band. The prepared sand sample was layered into the mold and compacted by a compactor. The filter paper, metal mesh, and water-permeable plate were then placed in the upper layer of the sand sample in-turn. Next, a two-way air intake cover was installed, and the sample was evacuated by a pump to detect the airtightness of the device. Afterward, the metal mold was removed and finally, the pressure chamber was closed with screws.

Water was injected into the confining pressure chamber, which slowly increased the pressure in the chamber via the booster pump, and simultaneously introduced methane gas into the sample chamber by means of the upper and lower two-way air intakes. This ensured the entire supercharging process. The pressure was always higher in the pressure chamber than in the sample chamber (i.e., the confining pressure was ~1.5–2.0 MPa higher than the pore pressure). Finally, the confining pressure was increased to 10 MPa, and the pore pressure was stopped at 9.0 MPa. The methane gas source was turned off, the sample chamber was connected to the buffer tank, the temperature of the system was maintained at 20 °C by a circulating water bath, and the sample was allowed to stand for 24 h to allow for sufficient inhalation. Thereafter, the temperature was adjusted to 5.0 °C for 48 h, before finally being adjusted to 2.0 °C for 48 h. The pore pressure of the sample was observed to judge whether or not the hydrate was completely formed.

After the hydrate had completely formed, the valve connected to the buffer tank in the sample chamber was closed. Low-temperature deionized water at ~2 °C was injected into the sample from the bottom of the sample chamber by a syringe pump, thereby draining the excess methane gas in the experiment, and changing the sample from a gas-saturated state to a water-saturated state. The remaining amount of free gas in the sample was judged by observing the gas–liquid separator at the bottom as the liquid content when the water discharge rate in the gas–liquid separator was essentially the same as the injection rate of the injection pump, and the volume of deionized water was used. When the pore volume of the sample had approximately doubled, the free gas was completely driven off by deionized water. In the process of water flooding, it was necessary to ensure that the pore pressure was lower than the experimentally required pore pressure of ~2.0 MPa, and that the pressure of the deionized water in the syringe pump was higher than the experimentally required pore pressure of ~1.0 MPa, but lower than the confining pressure. There was a pressure difference between the deionized water and the sample, such that the deionized water could be injected directly. After the water flooding process was completed, the pressure of the sample was increased using the syringe pump to the pressure required for the experiment, and the temperature was raised to 6.0 °C for the shear test.

2.3.2. Shearing and Decompression of Samples

The stress loading system was turned on and the shear rate was set to 0.20% per minute. The triaxial shearing process was divided into three stages. In the first stage, the axial strain rate was sheared from 0% to 2.2%. This stage represented undrained shear. When the axial strain rate reached ~2.2%, the axial load was unloaded and the shearing was stopped. Finally, the pore pressure was ~4.5 MPa, and liquid could be observed in the gas–liquid separator. Since the phase equilibrium pressure of methane hydrate at 6 °C is 4.73 MPa, the pore pressure of the sample was kept at 8.0 MPa during the shearing process in this stage, and the phase equilibrium condition was not destroyed. Therefore, the hydrate did not substantially decompose, and thus the amount of methane gas collected in the gas–liquid separator was extremely small. In this first stage, the pore pressure was finally reduced to ~4.5 MPa. Under the condition that the pore pressure was maintained at ~4.5 MPa and the temperature was 6.0 °C, the hydrate began to decompose slowly, and the methane gas (G_1) that decomposed after depressurization was collected and recorded.

In the second stage of shearing, the loading rate of the axial load remained consistent with the first stage, and the sample was retested under the new experimental parameters. The temperature during the shearing process was still 6.0 °C, and the pore pressure was ~4.5 MPa. In this stage, the axial strain rate was sheared from 2.2% to ~4.7%. The pore pressure was lower than with the phase equilibrium pressure of methane hydrate sediments at 6 °C, and the methane hydrate gradually began to decompose. However, since the pore pressure was slightly lower than the phase equilibrium pressure, the decomposition rate was slower. This stage still represented undrained shear. When the axial strain rate reached ~4.7%, the shearing was stopped, and the stress loading system was closed to unload the axial load. When the axial load was completely unloaded, the pressure relief valve that controlled the pore pressure was opened, and the pore pressure of the sample was gradually decreased to ~3.0 MPa. The pressure was much lower than the phase equilibrium pressure at 6.0 °C. Under the temperature and pressure conditions in this stage, the hydrate began to decompose in large amounts, and the collection rate of methane gas was much higher than in the first stage. After being decomposed into a gas, the pressure relief valve was closed, and the volume (G_2) of the methane gas generated by decomposition after pressure reduction was collected and recorded. The pressure relief valve was then closed, the axial load loading system was restored, and the third stage of shear testing was ready.

The third stage involved shearing of the axial strain rate from 4.7% to ~15%. The pore pressure at this stage was maintained at ~3.0 MPa, the system temperature was 6.0 °C, and the shear mode remained undrained. Since the pore pressure of the sample at this stage was much lower than the phase equilibrium pressure of the methane hydrate sediments at 6.0 °C, the methane hydrate in the sample was largely decomposed and the decomposition rate was faster than in previous stages. When the shear strain reached the axial strain rate of 15%, the shearing was stopped, the axial load was unloaded, the pressure relief valve was slowly opened, and the confining pressure and pore pressure of the system were gradually reduced to normal. The temperature also rose to 20 °C. After the methane hydrate in the hydrate sediments was completely decomposed and allowed to stand for one hour, the methane gas volume (G_0) generated by decomposition in all of the steps was collected and recorded; with this, the entire cutting process was complete. The difference between G_0 and G_2 is the sum of the remaining free gas and the gas generated after the decomposition of the remaining methane hydrate after the last stage. The specific experimental parameters of these tests are shown in Table 1.

Table 1. Sample parameters for shear experiments (Nos. 1–5).

Experiment No.	Clay Content (wt%)	Confining Pressure (MPa)	Pore Pressure (MPa)			Temperature (°C)	Saturation (%)		
			Stage 1	Stage 2	Stage 3		Stage 1	Stage 2	Stage 3
1	0	10	8	4.5	3	6	54.02	44.48	34.01
2	5	10	8	4.5	3	6	51.86	41.72	31.81
3	10	10	8	4.5	3	6	52.84	41.10	29.46
4	15	10	8	4.5	3	6	51.00	39.16	29.76
5	20	10	8	4.5	3	6	52.09	41.95	31.68

2.3.3. Calculation of Hydrate Saturation

Since the structure of natural gas hydrate is a non-metering cage structure, there is no way to express methane hydrate using a single, strict chemical formula, and thus the volume of methane hydrate containing a certain amount of methane gas will be not uniform. In this study, the saturation of methane hydrate (i.e., the methane hydrate in natural gas hydrate sediments) was calculated after the methods of Ghiassian et al. [30]. The theoretical basis of this method involves the assumption that a complete decomposition of methane hydrate per unit volume (1 m^3) releases ~160 units (m^3) of methane gas and an ~0.87 unit volume (m^3) of water. It is within this theoretical framework that the measurement of hydrate was considered, wherein the unit could be an ideal hydrate crystal. The specific formulae for this calculation can be seen in previous works [30].

3. Results and Discussion

3.1. Stress–Strain Relationship of Sediments with Different Clay Contents

The first stage shown in the curves of Figure 3 is the portion of the experiments with axial strain rates of 0–2.2%. At this stage, the stress–strain relationship was obtained when the sample pore pressure was 8 MPa and the confining pressure was 10 MPa (i.e., the effective confining pressure was 2 MPa). Since the pressure of the hydrate sediment sample at this stage was higher than the phase equilibrium pressure at the same temperature, the hydrate decomposition was minimal, and therefore the hydrate saturation of the sample was the highest. The stress–strain relationship at this stage reflects the initial stage of hydrate production.

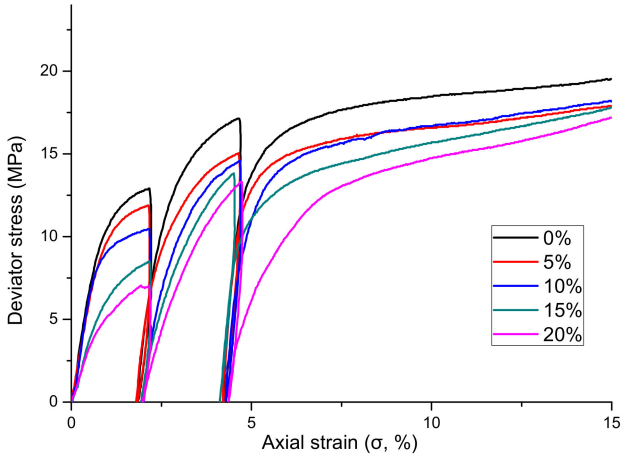

Figure 3. Stress–strain curves by clay content (%). The first stage represents axial strain rates of 0–2.2%, the middle stage accounts for rates of 2.2–4.7%, and the final arc represents strain rates of 4.7–15%. Different colors correspond to different clay contents.

It can be observed from Figure 3 that in the first stage of shearing, the stress–strain relationship between pure sand and sediments with different clay contents gradually changed from that of elastic to plastic strain. The samples initially exhibited elastic strain, indicating that they were not destroyed at the onset of shearing; when the applied stress was removed, the specimen could be restored to the original stress state. The reason for this may be that because the hydrate had not been decomposed, there were interactions between the sediment particles and the hydrate. Furthermore, because the effective confining pressure was low, the sediment particles were complete, and the particle skeleton did not change. Afterward, the elastic strain gradually changed to plastic strain, which indicates that the sample was broken, such that even if the axial load applied to the sample was removed, the sample could not be recovered. This may be due to some of the hydrate sediment particles moving under the action of the axial load and confining pressure, resulting in the cementation of the hydrate to the skeleton being destroyed and the hydrate sediment changing. At this stage, the hydrate was minimally decomposed, but due to the axial load, some of the hydrate was split, and these destroyed hydrates filled in between the hydrate sediment skeletons, making the entire sample more compact. Thus, the stress-strain relationship changed from one of elastic to plastic strain owing to changes in the skeleton and the failure of the destroyed hydrate particles. The first stage of shearing may be considered to have extended until an axial strain rate of ~2.7%, which was the maximum shear strength of the first stage. It can also be observed that the stress–strain relationships of sediments with different clay contents in the first stage differed, and the degree of plasticity gradually increased as the proportion of clay in the sediments increased. Additionally, as the clay content in the sediments increased, the strength of the hydrate sediments decreased.

The second stage shown in the curves of Figure 3 is for the experiments with axial strain rates of 2.2–4.7%. In this stage, the pore pressure was reduced from 8.0 MPa to 4.5 MPa, and the axial load was unloaded. After the hydrate in the sample was decomposed, the axial load system was restarted, and the effective confining pressure was kept at 10 MPa. Meanwhile, the stress–strain relationship was obtained by shearing under a confining pressure of 5.5 MPa. During the shearing process, the pressure of the hydrate sediment sample was slightly lower than the phase equilibrium pressure of the methane hydrate at 6.0 °C, and the hydrate also underwent partial decomposition. Since the hydrate had decomposed and exhaled part of the methane gas before shearing at this stage, the hydrate saturation of the sediment sample was lower than in the first stage of the experiments. In the second stage, during the exploitation of hydrates, the effective confining pressure of the hydrate sediments was greatly increased by depressurization, as the depressurized hydrate began to decompose.

The curve of the second stage represents the transformation from elastic to plastic strain (Figure 3). It can be observed from the stress–strain relationships of the second stage that the curve representing the same clay content had a substantially higher magnitude than during the first stage, which indicates that the strength of the second stage hydrate sediment was greater than that of the first stage. Since part of the water and methane gas in the sample were removed during the depressurization process before shearing, the hydrate sediment sample changed from a completely water-saturated state to an incompletely water-saturated state. The saturation was also lower than in the first stage. Under the same experimental conditions, the strength of water-saturated sediments was lower than that of the gas-saturated sediments, and as the abundance of hydrate sediments decreased, the methane hydrate sediments gradually decreased. The reason for this behavior may be that methane hydrate was formed between the sediment skeleton, and cemented the quartz sand skeleton, resulting in the higher strength of the methane hydrate sediment.

In the second stage of the experiments, the pore pressure of the hydrate sediments was greatly reduced, resulting in the effective confining pressure of the sample being much higher than in the first stage. Within a certain range of effective confining pressures, the strength of natural gas hydrate sediments will gradually increase with the increase of effective confining pressure. Based on the influencing factors described, it can be determined that for the methane hydrate sediments with different clay contents, the effects of the second-stage effective confining pressure and the change of hydrate sediments from water-saturated to partially water-saturated were less than that of the decreasing of hydrate saturation. More importantly, when comparing the curves of the first and second stages for the same clay content, it was found that the degree of elastic strain in the second stage was more obvious than that of plastic strain, and as the particle size of the sediments increased, the strength of the hydrate sediments also increased.

The third stage in the curves shown in Figure 3 corresponds to the part of the experiments with axial strain rates ranging from 4.7–15%, which reduced the pore pressure of the sample from 4.5 MPa to 3.0 MPa, and the effective confining pressure of this stage was 7.0 MPa. The resulting stress–strain relationship was obtained by shearing. The stress–strain relationship at this stage mainly changed from elastic to plastic strain, and finally to strain yielding. During the shearing process, the pressure of the hydrate sediment sample was much lower than the phase equilibrium pressure of the methane hydrate at 6.0 °C, at which time the hydrate in the sample was decomposed in large quantities and at a relatively fast rate. The hydrate saturation in the third stage was lower than in the first two stages, and a large volume of free water produced by the decomposition of the hydrate was also discharged. This stage simulated the middle and late stages of natural hydrate production. The hydrate had already been decomposed by a large amount, the gas hydrate sediment reservoir was greatly increased by the surrounding pressure, and the saturation of the hydrate in the reservoir was substantially reduced, resulting in hydrate sedimentation. The porosity of the sample also increased. As with the second stage, the hydrate saturation of the hydrate sediment sample was reduced due to the decomposition of the hydrate, and the decrease in the pore pressure caused the effective confining pressure of the sample to increase by 1.5 MPa relative to the second stage. However, comparing the curves of the

second and third stages, it can be seen that the curve in which the axial strain rate changed to 2.5% in the third stage is essentially the same as the curve in the second stage, which indicates that the effective confining pressure increased in this stage, yet the effect was small, and the influence on the mechanical properties of hydrate sediments was the same as for the decrease of hydrate saturation caused by decomposition. Therefore, no significant change in the strength of methane hydrate sediments was observed at this stage. Once the stress–strain relationships of the three stages were obtained, it was found that with the increase of the strain rate of triaxial compression, the stress–strain relationships of different particle sizes were gradually transformed into plastic strain. Ultimately, this became the strain yielding phenomenon, wherein the strain of the specimen could be recovered at the beginning; meanwhile, the structure of the specimen was gradually destroyed with the increasing of the axial load, and the damage became irreversible.

3.2. Strength Relationship of Sediments with Different Clay Contents

Figure 4 shows the relationship between the maximum shear strength of sediments with different clay contents and the ratio of clay to hydrate sediments from low to high. Maximum shear strength generally refers to the stress corresponding to the peak value of the stress–strain curve. However, in the case wherein the stress–strain curve has no significant peak value, the stress value at which the axial strain rate reached 15% was used. It can be seen from the figure that the maximum destructive strength of hydrate sediments was generally reduced as the proportion of clay in the sediment increased, and the maximum shear strength of the hydrate sediments of the pure sand skeleton was the highest. The reason for this may be that the strength of the material itself had a greater influence on the strength of the hydrate sediment. In general, the strength of clay is much lower than that of quartz sand. As the proportion of clay in the sediment increased, the content of quartz sand decreased correspondingly, such that the strength of the skeleton decreased. Additionally, some of the clay adhered to the surfaces of the sand grains, with some acting as a lubricant among the quartz sand particles, thereby reducing the cohesive force and internal friction, resulting in insufficient stability of the skeletal structure during the shearing process. The higher the clay content was, the more obvious this effect became.

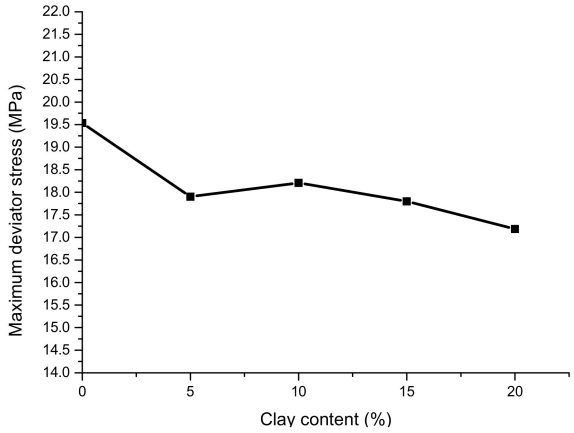

Figure 4. Maximum deviator stress by clay content (%).

The secant stiffness modulus E_{50} of sediments with different clay ratios is shown in Figure 5. This modulus is the line connecting the origin and 50% of the maximum shear strength in the stress–strain curve of the sediments. The slope of the line segment reflects the mean stiffness characteristics of the hydrate sediment. As is shown, when the hydrate content of the hydrate sediments increased under the same temperature and pressure conditions, the secant stiffness modulus gradually decreased. This reveals that as the clay content increased, the stiffness of the hydrate sediments gradually decreased.

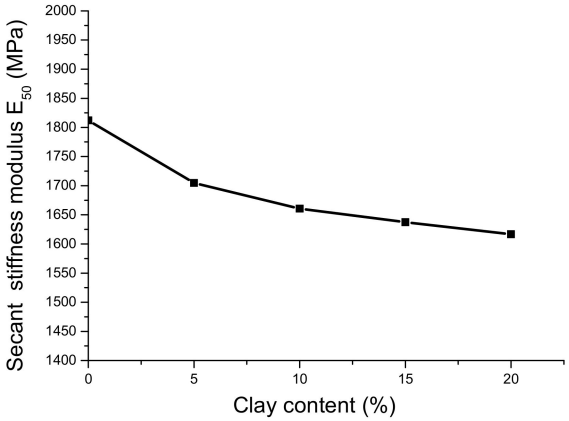

Figure 5. Secant stiffness modulus E_{50} of sediments by clay content (%).

In Figure 6, the initial tangential modulus E_0 of sediments with different clay ratios are shown. Under the same temperature and pressure conditions, the initial tangential modulus of sediments with different clay contents (as skeletons) also differed. As the clay content in the hydrate sediments increased, the initial tangential modulus of the hydrate sediments decreased gradually, while that of the pure sand (as the sediment skeleton) was the highest. Meanwhile, the initial tangential modulus of sediments with different clay contents was inconsistent. This may be due to the fact that the strength of clay is lower than that of quartz sand. The higher the clay content was in our experiments, the lower the proportion of quartz sand became. Moreover, the sediment skeletons with different clay contents were also different. The clay filled in the pores of the quartz sand skeleton, and the porosity with different clay contents also changed, which resulted in the cementation of the hydrate between the skeletons. In the same way, the initial strength of the entire hydrate sediment was decreased as the clay content increased.

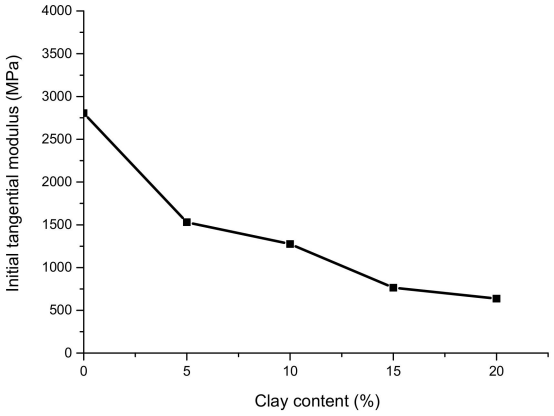

Figure 6. Initial tangential modulus of sediments by clay content (%).

3.3. Volumetric Strain Relationship of Sediments with Different Clay Contents

Figure 7 shows the volumetric strain curves for sediments with different clay proportions. It can be seen that in the first stage of shearing (i.e., when the axial strain rate was 0–2.2%), the volume of all hydrate sediment samples slightly increased as the strain rate increased and the magnitude of the change was maintained at ~0.5. The reason for this may be that in the first stage, the pore pressure of the experiment was always maintained at 8.0 MPa, which is higher than the equilibrium pressure of the phase, and the hydrate was hardly decomposed. Thus, the relationship between the hydrate and the sediment skeleton did not have much of an influence. This caused the hydrate sediment skeleton to not undergo much deformation. Additionally, the effective confining pressure at this stage

was always 2.0 MPa, and such a pressure condition was not enough to destroy the particles of the hydrate sediment. Therefore, the interaction between the particles and the relative position did not change much, which resulted in there being no significant change in the volume of the entire hydrate sediment sample.

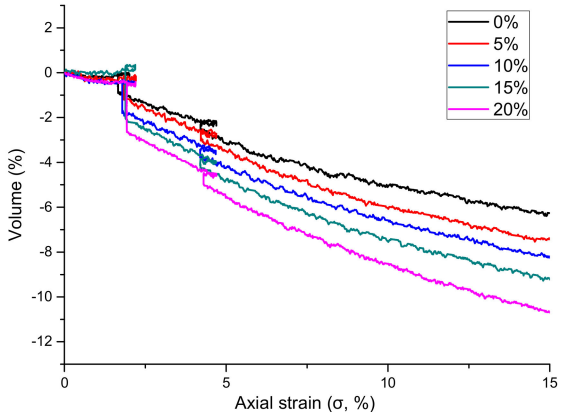

Figure 7. Volume–strain curves of sediments by clay content (%). The first stage represents axial strain rates of 0–2.2%, the middle stage accounts for rates of 2.2–4.7%, and the final stage represents strain rates of 4.7–15%. Different colors correspond to different clay contents.

In the second and third stages of the experiments, the axial strain rates were 2.2–4.7% and 4.7–15%, respectively, and the volume of hydrate sediments with different clay contents increased with the axial strain rate. With the reduction of hydrate content, an important clipping phenomenon occurred. The volumetric change in the second stage was generally >2.0%, while the shear shrinking phenomenon was more obvious in the third stage. The change in the volume of the sample with 20% clay content in the third stage even reached 5.0%. The reason for this may be that the pore pressures of the hydrate sediment samples in these two stages were lower than the phase equilibrium pressure of the hydrate at the same temperature, especially in the third stage. Thus, during the shearing process, the hydrate in the sample gradually decomposed, resulting in the formation of pores in the middle of the hydrate sediment skeleton. Under the influence of a certain effective confining pressure, some of the finer particles of clay filled the skeleton under the actions of the free water and gas generated by decomposition. Additionally, due to the large effective confining pressures in these two stages, some of the sediment particles may have been shredded. Under the external pressure, the shredded particles would have experienced larger positional changes, resulting in a change in the skeleton of the hydrate sediment sample, and ultimately in the volumetric reduction of the entire sample.

With the increase of clay content, the volumetric shearing effect of hydrate sediments became more obvious, likely because the strength of the clay was less and its compressibility was higher than that of the quartz sand. Therefore, as the clay content increased, the volume became more compressed. Figure 8 shows the grain size curve of the sediments before and after the triaxial compressive shearing of 40–60 μm specimens. It can be seen from this figure that the particle sizes before shearing were larger than afterward. This means that after shearing, the higher effective confining pressure and axial load became part of the sand. Additionally, the volume of the hydrate sediment sample suddenly declined each time the axial load pressure was unloaded during the experiment. This may have been due to the fact that these two stages comprised a process of hydrate decomposition and drainage. First, the depressurized hydrate was decomposed, and a certain amount of gas and the free water generated by decomposition were discharged, such that many pores were generated among the hydrate sediment samples. Moreover, in the process of free water and gas discharge, sand and clay also underwent substantial displacement under the movement of the free water and methane gas, which could have significantly changed the skeletal structure of hydrate sediments, especially when they were not

decomposed. Finally, the sediment skeleton played a very important role in cementation, and the originally fixed skeleton was destroyed after decomposition; because of the increase in the effective confining pressure, the compression of the sample became more pronounced.

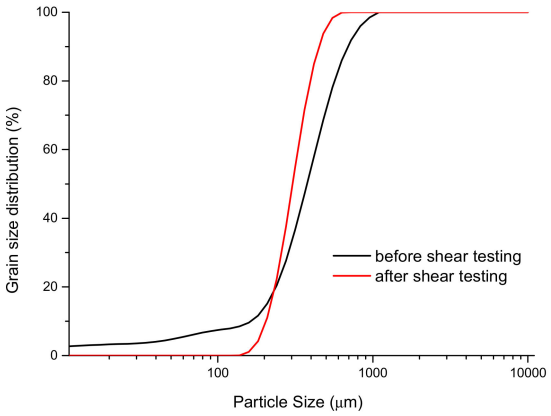

Figure 8. Grain size distribution curves of 40–60 mesh particle sizes before (black line) and after (red line) shear testing.

4. Conclusions

The stress–strain relationship of hydrate sediments containing clay (kaolin) during shearing is mainly divisible into three stages, namely elastic strain, plastic strain, and the strain yielding stage. In multi-stage triaxial shear tests with discontinuous depressurization, the mechanical strength varied with hydrate decomposition. With the increase of the axial strain rate under triaxial compression, all experiments showed that the elastic strain was gradually transformed into plastic strain. During the course of these experiments, the strain yielding phenomena changed, which indicates that the strain of the specimen could be restored at the beginning, but with the progressive loading of the axial load, the structure of the specimen was gradually destroyed, and the damage became irreversible.

The proportion of clay in the methane sediment affected the mechanical strength of the hydrate sediment sample. This may have been because the clay particles were smaller and could fill the pores of the coarser sediment skeleton, while the clay offered less support to the skeleton, and the hydrate more strongly cemented the skeleton with increasing clay content. As the proportion of clay increased, the strength of the entire sample gradually decreased. The clay also affected the volumetric strain during methane hydrate shearing. Regardless of the amount of clay added, the hydrate sediments shrank, but as the hydrates gradually decomposed, the shrinkage of the sediments became more pronounced as the clay content increased. The reason for this may be that the strength of the clay was less than that of the quartz sand, and the change in volume during the shearing process was greater than that of the quartz sand. As the hydrate decomposed, the pores between the quartz sand skeletons gradually increased, and the smaller clay particles filled the pores of the skeleton under the external shearing force, thereby causing the shearing behavior observed.

Author Contributions: D.L. (Dongliang Li), D.L. (Deqing Liang), and X.W. conceived and designed the experiments; Z.W. performed the experiments; D.L. (Dongliang Li) and Z.W. analyzed the data and wrote the paper.

Funding: This work was supported by the National Natural Science Foundation of China (grant nos. 51661165011, 51474197 and 41674076), the National Key Research & Development Plan of China (grant no. 2017YFC0307305), the Guangdong Province MEDProject (grant no. GDME-2018D002), and the Natural Science Foundation of Guangdong Province (grant no. 2018B0303110007).

Conflicts of Interest: The authors declare no conflict of interest.

References

1. Sloan, E.D. *Clathrate Hydrates of Natural Gas*, 2nd ed.; CRC Press: Boca Raton, FL, USA, 1998.
2. Klauda, J.B.; Sandler, S.I. Global distribution of methane hydrate in ocean sediment. *Energy Fuels* **2005**, *19*, 459–470. [CrossRef]
3. Collett, T.S. Energy resource potential of natural gas hydrates. *AAPG Bull.* **2002**, *86*, 1971–1992.
4. Milkov, A.V. Global estimates of hydrate-bound gas in marine sediments: How much is really out there? *Earth-Sci. Rev.* **2004**, *66*, 183–197. [CrossRef]
5. Li, G.; Li, X.S.; Tang, L.G.; Zhang, Y. Experimental investigation of production behavior of methane hydrate under ethylene glycol injection in unconsolidated sediment. *Energy Fuels* **2007**, *21*, 3388–3393. [CrossRef]
6. Tang, L.G.; Li, X.S.; Feng, Z.P.; Li, G.; Fan, S.S. Control mechanisms for gas hydrate production by depressurization in different scale hydrate reservoirs. *Energy Fuels* **2007**, *21*, 227–233. [CrossRef]
7. Komatsu, H.; Ota, M.; Smith, R.L.; Inomata, H. Review of CO_2–CH_4 clathrate hydrate replacement reaction laboratory studies – Properties and kinetics. *J. Taiwan Inst. Chem. Eng.* **2013**, *44*, 517–537. [CrossRef]
8. Kwon, T.-H.; Cho, G.-C. Submarine Slope failure primed and triggered by bottom water warming in oceanic hydrate-bearing deposits. *Energies* **2012**, *5*, 2849–2873. [CrossRef]
9. Gan, H.Y.; Wang, J.S.; Hu, G.W. Submarine Landslide Related to Natural Gas Hydrate within Benthal Deposit. *J. Seismol.* **2004**, *24*, 117–181.
10. Winters, W.; Walker, M.; Hunter, R.; Collett, T.; Boswell, R.; Rose, K.; Waite, W.; Torres, M.; Patil, S.; Dandekar, A. Physical properties of sediment from the Mount Elbert Gas Hydrate Stratigraphic Test Well, Alaska North Slope. *Mar. Pet. Geol.* **2011**, *28*, 361–380. [CrossRef]
11. Winters, W.; Waite, W.; Mason, D.; Gilbert, L.; Pecher, I.; Waite, W. Methane gas hydrate effect on sediment acoustic and strength properties. *J. Pet. Sci. Eng.* **2007**, *56*, 127–135. [CrossRef]
12. Hyodo, M.; Nakata, Y.; Yoshimoto, N.; Ebinuma, T. Basic Research on the mechanical behavior of methane hydrate-sediments mixture. *J. Jpn. Geotech. Soc. Soils Found.* **2005**, *45*, 75–85.
13. Hyodo, M.; Li, Y.; Yoneda, J.; Nakata, Y.; Yoshimoto, N.; Nishimura, A.; Song, Y. Mechanical behavior of gas-saturated methane hydrate-bearing sediments. *J. Geophys. Res. Solid Earth* **2013**, *118*, 5185–5194. [CrossRef]
14. Hyodo, M.; Wu, Y.; Nakashima, K.; Kajiyama, S.; Nakata, Y. Influence of fines content on the mechanical behavior of methane hydrate-bearing sediments. *J. Geophys. Res. Solid Earth* **2017**, *122*, 7511–7524. [CrossRef]
15. Li, Y.; Song, Y.; Yu, F.; Liu, W.; Wang, R. Effect of confining pressure on mechanical behavior of methane hydrate-bearing sediments. *Pet. Explor. Dev.* **2011**, *38*, 637–640. [CrossRef]
16. Li, Y.; Song, Y.; Liu, W.; Yu, F. Experimental research on the mechanical properties of methane hydrate-ice mixtures. *Energies* **2012**, *5*, 181–192. [CrossRef]
17. Song, Y.; Yu, F.; Li, Y.; Liu, W.; Zhao, J. Mechanical property of artificial methane hydrate under triaxial compression. *J. Nat. Gas Chem.* **2010**, *19*, 246–250. [CrossRef]
18. Song, Y.; Zhu, Y.; Liu, W.; Zhao, J.; Li, Y.; Chen, Y.; Shen, Z.; Lu, Y.; Ji, C. Experimental research on the mechanical properties of methane hydrate-bearing sediments during hydrate dissociation. *Mar. Pet. Geol.* **2014**, *51*, 70–78. [CrossRef]
19. Masui, A.; Haneda, H.; Ogata, Y.; Aoki, K. Effects of methane hydrate formation on shear strength of synthetic methane hydrate sediments. In Proceedings of the Fifteenth International Offshore and Polar Engineering Conference, Seoul, Korea, 19–24 June 2005.
20. Miyazaki, K.; Masui, A.; Sakamoto, Y.; Aoki, K.; Tenma, N.; Yamaguchi, T. Triaxial compressive properties of artificial methane-hydrate-bearing sediment. *J. Geophys. Res. Space Phys.* **2011**, *116*, 6. [CrossRef]
21. Kajiyama, S.; Wu, Y.; Hyodo, M.; Nakata, Y.; Nakashima, K.; Yoshimoto, N. Experimental investigation on the mechanical properties of methane hydrate-bearing sand formed with rounded particles. *J. Nat. Gas Sci. Eng.* **2017**, *45*, 96–107. [CrossRef]
22. Hyodo, M.; Li, Y.; Yoneda, J.; Nakata, Y.; Yoshimoto, N.; Nishimura, A. Effects of dissociation on the shear strength and deformation behavior of methane hydrate-bearing sediments. *Mar. Pet. Geol.* **2014**, *51*, 52–62. [CrossRef]
23. Jang, J.; Santamarina, J.C. Hydrate bearing clayey sediments: Formation and gas production conepts. *Mar. Pet. Geol.* **2016**, *77*, 235–246. [CrossRef]
24. Boswell, R. Is Gas Hydrate Energy Within Reach? *Science* **2009**, *325*, 957–958. [CrossRef] [PubMed]

25. Boswell, R.; Collett, T.S. Current perspectives on gas hydrate resources. *Energy Environ. Sci.* **2011**, *4*, 1206–1215. [CrossRef]
26. Dai, S.; Lee, C.; Santamarina, J.C. Formation history and physical properties of sediments from the Mount Elbert Gas Hydrate Stratigraphic Test Well, Alaska North Slope. *Mar. Pet. Geol.* **2011**, *28*, 427–438. [CrossRef]
27. Li, Y.; Hu, G.; Wu, N.; Liu, C.; Chen, Q.; Li, C. Undrained shear strength evaluation for hydrate-bearing sediment overlying strata in the Shenhu area, northern South China Sea. *Acta Oceanol. Sin.* **2019**, *38*, 114–123. [CrossRef]
28. Choi, J.H.; Dai, S.; Lin, J.S.; Seol, Y. Multi-stage triaxial tests on laboratory-formed methane hydrate-bearing sediments. *J. Geophys. Res. Solid Earth* **2018**, *123*, 3347–3357. [CrossRef]
29. Li, D.; Wu, Q.; Wang, Z.; Lu, J.; Liang, D.; Li, X. Tri-axial shear tests on hydrate-bearing sediments during hydrate dissociation with depressurization. *Energies* **2018**, *11*, 1819. [CrossRef]
30. Ghiassian, H.; Grozic, J.L. Strength behavior of methane hydrate bearing sand in undrained triaxial testing. *Mar. Pet. Geol.* **2013**, *43*, 310–319. [CrossRef]